Feedback control of flow alignment in sheared liquid crystals

David A. Strehober,[*] Eckehard Schöll, and Sabine H. L. Klapp[†]

Institut für Theoretische Physik, Sekretariat EW 7-1, Technische Universität Berlin, Hardenbergstraße 36, D-10623 Berlin, Germany

Based on a continuum theory, we investigate the manipulation of the nonequilibrium behavior of a sheared liquid crystal via closed-loop feedback control. Our goal is to stabilize a specific dynamical state, that is, the stationary "flow alignment," under conditions where the uncontrolled system displays oscillatory director dynamics with in-plane symmetry. To this end we employ time-delayed feedback control (TDFC), where the equation of motion for the ith component $q_i(t)$ of the order parameter tensor is supplemented by a control term involving the difference $q_i(t) - q_i(t - \tau)$. In this diagonal scheme, τ is the delay time. We demonstrate that the TDFC method successfully stabilizes flow alignment for suitable values of the control strength K and τ; these values are determined by solving an exact eigenvalue equation. Moreover, our results show that only small values of K are needed when the system is sheared from an isotropic equilibrium state, contrary to the case where the equilibrium state is nematic.

I. INTRODUCTION

Liquid crystals under shear can display a variety of nonequilibrium dynamical states determining the motion of the director of the (shear-induced or spontaneous) orientational ordering. The simplest of these states is the stationary "flow alignment" typically occurring at large shear rates and/or large values of the (particle geometry-related) coupling parameter λ_K. However, the systems can also display various types of oscillatory motion, spatiotemporal symmetry breaking, and even chaotic behavior [1–6]. The discovery of this rich dynamical behavior has stimulated intense research both by theoretical methods (such as continuum approaches [7–11] and particle-based computer simulations [5,12–14]) and by experiments (see, e.g., [15,16]).

The nonlinear orientational dynamics also has direct implications for the rheological behavior of the system as reflected, e.g., by nonmonotonic stress-strain curves ("constitutive relations") [17–23] and a non-Newtonian behavior of the viscosity. Understanding the dynamics is thus a prerequisite for the deliberate design of materials with specific rheological properties, which are tunable by parameters such as particle geometry, concentration (temperature), and external fields.

Beyond pure understanding, however, one may wish to *stabilize* a certain dynamic state with a well-defined associated rheology. A candidate for stabilization could be the stationary shear-alignment state. Indeed, it has been shown [22,24] that the viscosity in such a state is particularly low ("shear thinning"), in fact, lower than the viscosity of the corresponding unsheared system. In other words the stationary alignment of the liquid crystal molecule in the shear flow tends to lower frictional effects. This situation changes dramatically when the nematic director starts to oscillate [22]. Thus, shear-aligned systems may serve as particularly good lubricants.

In this paper we investigate the possibility to stabilize the flow-aligned state by a continuum approach for the orientational dynamics [7,8], combined with the method of time-delayed feedback control (TDFC). The relevant dynamical variable within the continuum approach is the second-rank alignment tensor $\mathbf{a}(t)$ carrying five independent components. In a previous short study [25] we have already shown the TDFC to be successful if the dynamics of the full $\mathbf{a}(t)$ is simplified into that of a two-dimensional director characterizing uniaxial, shear-induced ordering within the shear plane. In the present paper we release this somewhat artificial restriction and investigate the full (in-plane) dynamics under TDFC. We focus on conditions where the uncontrolled system displays a wagging-like oscillatory motion within the shear plane. In this situation it seems tempting to consider only a reduced (three-dimensional) system involving only those components of the order parameter $\mathbf{a}$ which describe in-plane dynamics. However, as it was demonstrated in previous studies [2,26], this reduction can predict a stable fixed point (the so-called log rolling) which is actually unstable after inclusion of the remaining components of the order parameter. We thus consider the full five-dimensional dynamical system to explore stability.

As in our earlier work [27], we did make some simplifying assumptions. First, we do not consider back coupling of the orientational dynamics onto the flow. Rather, we assume that the velocity field is imposed externally. Extensions of the theory incorporating such effects are proposed in a study by Lima and Rey [28] as well as one by Heidenreich *et al.* [23]. Second, we neglect the role of boundaries, which was discussed by Tsuji and Rey [29] as well as in [23]. A third assumption is that we consider our sheared system to be free of defects (for corresponding extensions, see [30]). Moreover, in the context of TDFC, we explore the interplay between the performance of the control scheme, on the one hand, and the nature of the underlying equilibrium phase from which the liquid crystal is sheared, on the other hand. TDFC is a closed-loop control method proposed by Pyragas [31], which allows one to stabilize periodic and steady states which would be unstable otherwise. In the meantime, TDFC has been applied to a broad variety of nonlinear systems, including semiconductor nanostructures [32–35], lasers [36,37], excitable media [38–40], and neural systems [41–43] (see [44,45] for overviews). Within the Pyragas method, the equations

---

[*]physik@strehober.de

[†]klapp@physik.tu-berlin.de

of motion are supplemented by control terms built on the differences $q_i(t) - q_i(t - \tau)$ between the present and an earlier value of an appropriate system variable q_i. This type of control is noninvasive as the control forces vanish when the steady state (or a periodic state with period $T = n\tau$, with $n = 1,2,3,\ldots$) is reached. A general, analytic investigation of the application of TDFC to steady states has been given in Ref. [46].

This paper is organized as follows. We start in Sec. II with a review of the basic dynamical equations for the order parameter $\boldsymbol{a}(t)$. In Sec. III A we summarize the dynamical behavior occurring that depends on the shear rate and the coupling parameter for two temperatures (and, correspondingly, different phases) of the underlying equilibrium system (for a full discussion based on a bifurcation analysis, see Ref. [27]. For each reduced temperature θ, we select a parameter set in which the uncontrolled system displays oscillatory director dynamics within the shear plane. The theoretical background of the TDFC method is introduced in Sec. III B. Numerical results for the selected parameter sets are presented in Sec. IV. Finally, we give a conclusion and outlook.

II. BACKGROUND: CONTINUUM THEORY OF THE ORIENTATIONAL DYNAMICS UNDER SHEAR

We employ a mesoscopic description of the system, where the relevant dynamic variable is the orientational order parameter averaged over some volume in space. In a sheared liquid crystal, this order parameter corresponds to the time-dependent, second-rank alignment tensor $\mathbf{a} = \sqrt{15/2}\langle \overline{\mathbf{uu}} \rangle$, where $\mathbf{u}$ describes the orientation of the molecular axis and $\overline{\cdots}$ indicates the symmetric traceless part of a tensor. The average $\langle \ldots \rangle$ is defined as (see Ref. [27])

$$\langle \cdots \rangle = \int_{S^2} d^2\boldsymbol{u} \, \ldots \, \rho^{\text{or}}(\boldsymbol{u},\boldsymbol{r},t), \qquad (2.1)$$

involving the orientational distribution function $\rho^{\text{or}}(\boldsymbol{u},\boldsymbol{r},t)$ [47]. The integral in Eq. (2.1) is performed over the unit sphere. The orientational distribution is defined as $\rho^{\text{or}}(\boldsymbol{u},\boldsymbol{r},t) = N^{-1}\langle \sum_{i=1}^{N} \delta(\boldsymbol{u} - \boldsymbol{u}_i(t)) \rangle_{\text{ens}}$, where $\boldsymbol{u}_i$ is the microscopic orientation of particle i ($i = 1,\ldots,N$) and $\langle \ldots \rangle_{\text{ens}}$ is an ensemble average in a small volume dV around the space point $\boldsymbol{r}$ at time t.

In the isotropic equilibrium state, all components of $\mathbf{a}$ are zero, whereas nematic ordering (which may be uniaxial or biaxial in character) is characterized by one or several components of $\mathbf{a}$ being nonzero.

Switching on an external shear flow characterized by a velocity field $\mathbf{v}$, the alignment tensor becomes a time-dependent quantity. Its equation of motion can be derived from a generalized Fokker-Planck equation [8–10] or, alternatively, from irreversible thermodynamics [7], yielding for a homogeneous system (in dimensionless form) [48]

$$\frac{d\mathbf{a}}{dt} = 2\,\overline{\boldsymbol{\Omega} \cdot \mathbf{a}} + 2\sigma\,\overline{\boldsymbol{\Gamma} \cdot \mathbf{a}} - \Phi'(\boldsymbol{a}) + \sqrt{\frac{3}{2}}\lambda_{\text{K}}\,\boldsymbol{\Gamma}. \quad (2.2)$$

In Eq. (2.2), $\boldsymbol{\Gamma} = [(\nabla\mathbf{v})^T + \nabla\mathbf{v}]/2$ is the strain rate tensor (with the superscript T denoting the transpose of tensor $\nabla\mathbf{v}$) and $\boldsymbol{\Omega} = [(\nabla\mathbf{v})^T - \nabla\mathbf{v}]/2$ is the vorticity. The symbol $\overline{\mathbf{x}}$ indicates the symmetric traceless part of a tensor $\mathbf{x}$,

i.e., $\overline{\mathbf{x}} = 1/2(\mathbf{x} + \mathbf{x}^T) - 1/3 Tr(\mathbf{x})$. In the present work we consider a planar Couette flow characterized by $\mathbf{v} = \dot{\gamma}y\mathbf{e}_{\text{x}}$, with $\dot{\gamma}$ being the shear rate and $\mathbf{e}_{\text{x}}$ being a unit vector. This yields $\boldsymbol{\Gamma} = \dot{\gamma}\,\overline{\mathbf{e}_{\text{x}}\mathbf{e}_{\text{y}}}$ and $\boldsymbol{\Omega} = (\dot{\gamma}/2)(\mathbf{e}_{\text{x}}\mathbf{e}_{\text{y}} - \mathbf{e}_{\text{y}}\mathbf{e}_{\text{x}})$, respectively. The (dimensionless) parameter λ_{K} is the so-called tumbling parameter, which measures the coupling strength between alignment and strain. This parameter is related to the shape (i.e., the aspect ratio) of the particles [8]. The relaxation parameter σ plays only a minor role, and following previous works [1,27,49–51], we set $\sigma = 0$. Finally, the (tensorial) quantity $\Phi'(\boldsymbol{a})$ appearing in Eq. (2.2) corresponds to the derivative of the free energy with respect to the (nonconserved) order parameter, i.e., $\Phi'(\boldsymbol{a}) = \partial\Phi/\partial\mathbf{a}$. We employ the (dimensionless) Landau–de Gennes (LG) expression for the free energy [52] given by

$$\Phi = \frac{\theta}{2}\mathbf{a} : \mathbf{a} - \sqrt{6}\,(\mathbf{a} \cdot \mathbf{a}) : \mathbf{a} + \frac{1}{2}\,(\mathbf{a} : \mathbf{a})^2, \qquad (2.3)$$

where the notation ":" stands for the trace over the product of two tensors and "·" indicates conventional matrix multiplication. In Eq. (2.3), θ plays the role of an effective, dimensionless temperature, which is the tuning parameter for the isotropic-nematic transition in thermotropic liquid-crystal systems. A first-order isotropic-nematic transition occurs at $\theta = 1$. For temperatures $\theta > 1$ ($\theta < 1$) the isotropic (nematic) phase is stable, i.e., it corresponds to the lowest minimum of the free energy. Upon "cooling down" from high temperatures, the nematic state appears as a metastable phase already at $\theta = 9/8$. Crossing the phase transition (at $\theta = 1$), the isotropic phase remains as a metastable phase down to $\theta = 0$, below which it becomes unstable. We note that this general scenario applies not only to thermotropic liquid crystals (where θ is related to a true temperature) but also to lyotropic liquid crystals and suspensions of colloidal rods. In these cases, the isotropic-nematic transition is triggered by the concentration, and θ has to be defined accordingly [27]; otherwise, the approach remains the same.

Equation (2.2) is most conveniently solved by expanding $\boldsymbol{a}$ and the other tensors appearing on the right side into a tensorial basis set (see, e.g., [2]), e.g., $\boldsymbol{a} = \sum_{l=0}^{4} a_l \mathbf{T}^l$, where a_l are the (five) independent components of $\mathbf{a}$ and the (orthonormal) tensors $\mathbf{T}^l$ involve linear combinations of the unit vectors $\mathbf{e}_{\text{x}}$, $\mathbf{e}_{\text{y}}$, and $\mathbf{e}_{\text{z}}$ (for explicit expressions, see, e.g., Ref. [2]). One then obtains the five-dimensional dynamical system

$$\dot{\boldsymbol{q}} = \boldsymbol{F}, \qquad (2.4)$$

where the vector $\boldsymbol{q} = (a_0,a_1,a_2,a_3,a_4)$ and the components of the vector $\boldsymbol{F}$ are given by

$$\begin{aligned}
F_0 &= -\phi_0, \\
F_1 &= -\phi_1 + \dot{\gamma}a_2, \\
F_2 &= -\phi_2 - \dot{\gamma}a_1 + \tfrac{1}{2}\sqrt{3}\lambda_K\dot{\gamma}, \\
F_3 &= -\phi_3 + \tfrac{1}{2}\dot{\gamma}a_4, \\
F_4 &= -\phi_4 - \tfrac{1}{2}\dot{\gamma}a_3.
\end{aligned} \qquad (2.5)$$

In Eqs. (2.5), the quantities ϕ_l ($l = 0,\ldots,4$) represent the components of the vector $\boldsymbol{\Phi}$ [which consist of the projections of $\Phi'(\boldsymbol{a})$ on the tensor basis]. These quantities are nonlinear

functions of a_l; explicit expressions are given in the Appendix.

III. FEEDBACK CONTROL

A. Choosing candidate states

The dynamical behavior emerging from the mesoscopic equations of motion (2.4) has been studied in detail for a variety of temperatures θ (determining the behavior of the unsheared system) and a broad range of shear rates $\dot{\gamma}$ and shear coupling parameters λ_K [1,2,26,27,49,53]. In particular in Ref. [27], we have investigated systems at different temperatures via a numerical bifurcation analysis (for numerical details, see the Appendix of [27]). Special attention has been devoted to systems sheared from the stable or metastable nematic equilibrium phase ($\theta \leqslant 9/8$). An exemplary dynamical state diagram for the case $\theta = 0$ is shown in Fig. 1 (data taken from Ref. [27] and the diagram are consistent with earlier works, i.e., [1,2,26]).

For large values of the shear rate ($\dot{\gamma} \gtrsim 4.5$, i.e., above the semicircle line in Fig. 1) the stable dynamical states have in-plane symmetry. In this case the main director is restricted to directions within the shear plane (i.e., the x-y plane), implying that the components $a_3 = a_4 = 0$. At large values
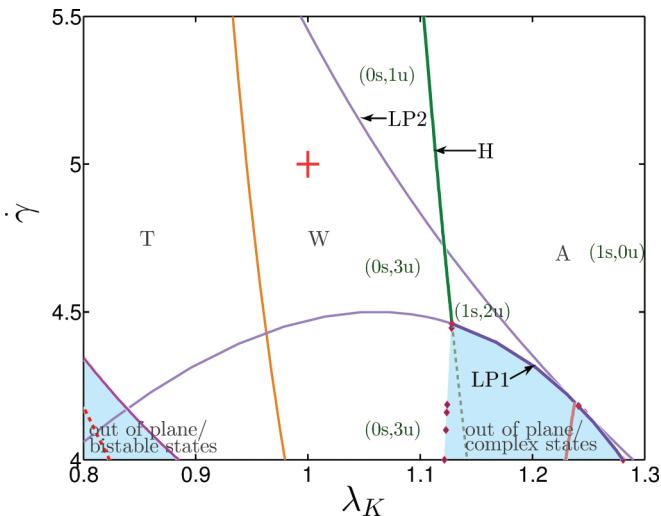

FIG. 1. (Color online) Dynamical state diagram in the plane spanned by the tumbling parameter λ_K and the (dimensionless) shear rate $\dot{\gamma}$ for a nematic system ($\theta = 0$). The lines were obtained via a codimension-2 bifurcation analysis as described in Ref. [27]. The nearly vertical line represents a supercritical Hopf bifurcation line (H). On the right side of the H line we find flow alignment (A), corresponding to a stable fixed point. This is indicated by the notation (1s,0u), where 1s and 0u mean one stable (s) and no unstable (u) fixed point, respectively. Upon crossing the H line towards lower values of λ_K, oscillatory in-plane states [wagging (W) and tumbling (T)] become stable. As indicated by the notation (0s,3u) [and (0s,1u)] there is no stable fixed point in this area, but three (one) unstable ones. The cross marks the parameter set $\boldsymbol{\beta}_I = (\lambda_K = 1.0, \dot{\gamma} = 5.0, \theta = 0)$ where we apply feedback control. The shaded areas appearing at low $\dot{\gamma}$ correspond to oscillatory states with out-of-plane symmetry. The lines labeled LP1 and LP2 are limit point lines (saddle-node bifurcation lines).

of the coupling parameter λ_K, this in-plane state is stationary in character, reflecting that the nematic director is "frozen" and encloses a fixed angle with the direction of the shear flow. This is the so-called flow-alignment state, which we label by A. Mathematically, the A state corresponds to a stable fixed point of the dynamics. Decreasing the coupling parameter λ_K (at fixed, large $\dot{\gamma}$), one encounters a supercritical Hopf bifurcation [27], and the system displays oscillatory states with in-plane symmetry. These are the so-called wagging (W) state, occurring at intermediate values of λ_K, and tumbling (T) state, occurring at low λ_K. Both T and W are characterized by the presence of stable limit cycles and, correspondingly, unstable fixed points (for a more detailed discussion, see Sec. IV). In the W state the angle between the nematic director and the flow direction oscillates periodically between a minimal and a maximal value, whereas in the T state, the director performs full, in-plane rotations. We stress, however, that there is no fundamental difference between W and T motion in the sense that these states are not separated by a bifurcation [27].

At lower shear rates, additional dynamical states appear which are characterized by nonzero values for all five components of the order parameter. Physically, this means that the main director performs oscillations not only within the shear plane but also out of this plane. Typical representatives are the "kayaking wagging" (KW) and "kayaking tumbling" (KT) states first observed in Ref. [54]. In Fig. 1, such out-of-plane solutions occur in the shaded regions. We have also indicated regions of bistability and complex chaotic behavior (for a more detailed discussion, see Refs. [1,2,26,27]).

The main goal of the present paper is to explore the stabilization of the fixed point corresponding to flow alignment within a parameter range where the system is in an *in-plane* oscillatory state (i.e., W or T). The specific position in parameter space is indicated by the cross in Fig. 1, corresponding to the parameter set $\boldsymbol{\beta}_I := (\lambda_K = 1.0, \dot{\gamma} = 5.0, \theta = 0)$.

Our reasoning for focusing on in-plane situations is twofold: First, the absence of stable out-of-plane solutions allows us to focus on only three components of the order parameter tensor, that is, a_0, a_1, and a_2. Second, it has been shown [27] that the out-of-plane states do *not* arise via a Hopf bifurcation. Thus, there is no "natural" unstable fixed point which one could try to stabilize via TDFC.

In addition to a nematic system, we also consider in our study a system which is *isotropic* in the absence of shear ($\theta = 1.20$). A corresponding state diagram is shown in Fig. 2. At large coupling parameters ($\lambda_K \gtrsim 0.75$), the shear flow induces first ($\dot{\gamma} \lesssim 0.2$) a "paranematic" ordering characterized by very small values of the order parameters. With increasing $\dot{\gamma}$, the system then transforms via a first-order transition into a flow-aligned state (A). Interestingly, however, the system can also display an in-plane oscillatory state, that is, wagging (W). This behavior is rather surprising in view of the isotropic nature of the underlying equilibrium state and was detected only recently [27]. As seen from Fig. 2, the wagging occurs in a parameter island located at lower values of λ_K. The major part of the boundaries of this island represent Hopf bifurcations. We select a parameter point within this wagging island as a second candidate for feedback control. Specifically, $\boldsymbol{\beta}_{II} := (\lambda_K = 0.6, \dot{\gamma} = 0.8, \theta = 1.20)$.
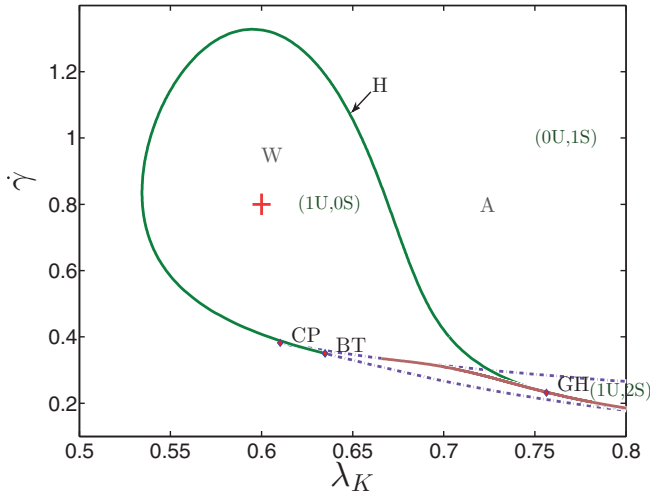
FIG. 2. (Color online) Dynamical state diagram at $\theta = 1.20$, where the unsheared system is isotropic. The lines are obtained via a codimension-2 bifurcation analysis as described in Ref. [27]. With the bifurcation analysis we also detect special points like the cusp point (CP), Bogdanov-Takens point (BT), and generalized Hopf point (GH). The solid line (shaped like an oval) represents a supercritical H bifurcation line, within which the system is in an oscillatory (W) state. The cross marks the parameter set $\boldsymbol{\beta}_{\mathrm{II}} = (\lambda_K = 0.6, \dot{\gamma} = 0.8, \theta = 1.20)$ selected as a second candidate for feedback control. Outside this W regime (characterized by one unstable fixed point), the system is in a stationary, flow-aligned state (A). The dashed lines appearing in the bottom right corner of the diagram are limit point lines (LP) (saddle-node bifurcation lines). Between the LP curves one finds areas of bistability between paranematic and nematic states (for details on that, see Ref. [27]). The notation regarding the fixed points is as in Fig. 1.

Having identified suitable parameter sets ($\boldsymbol{\beta}_{\mathrm{I}}, \boldsymbol{\beta}_{\mathrm{II}}$) that apply feedback control of steady states, we now turn to a detailed discussion of (i) the stability of the corresponding steady states and (ii) their behavior under TDFC with a diagonal control scheme. The corresponding methods are outlined in the Sec. III B. In Sec. IV, we will present the numerical results.

As already remarked in the Introduction, we perform the stability analysis described below with the full, five-dimensional system (see also discussion in Sec. IV A). In this way we avoid difficulties arising if one considers the three-component system alone.

B. Time-delayed feedback control

As a starting point for feedback control, we first need to determine the steady states (fixed points) $\boldsymbol{q}^{\star} = (a_0^{\star}, a_1^{\star}, a_2^{\star}, a_3^{\star}, a_4^{\star})$ of the dynamical system [see Eq. (2.4)] corresponding to the two parameter sets $\boldsymbol{\beta}_{\mathrm{I}}, \boldsymbol{\beta}_{\mathrm{II}}$. The fixed points fulfill the condition $\dot{\boldsymbol{q}}^{\star} = 0$. We have solved these equations numerically.

For each fixed point, its linear stability can be checked by considering the 5×5 Jacobian $\mathbf{J}$ of the dynamical system. The elements $J_{ij} = \partial F_i / \partial q_j$ of $\mathbf{J}$ are given in the Appendix. Small perturbations $\delta \mathbf{q}(t)$ away from the steady state evolve with time as $\dot{\delta \mathbf{q}}(t) = \mathbf{J} \delta \mathbf{q}(t)$. This linear equation can be solved with the ansatz $\delta \mathbf{q}(t) = \mathbf{A} \exp[\nu t]$ (with $\mathbf{A}$ containing the real amplitudes of the perturbation), yielding the eigenvalue

equation

$$\nu \delta \mathbf{q} = \mathbf{J} \delta \mathbf{q}. \tag{3.1}$$

The eigenvalues can then be calculated from the characteristic equation $\det(\mathbf{J} - \nu \mathbf{I}) = 0$ (where $\mathbf{I}$ is the unity matrix). Stability of the fixed point $\boldsymbol{q}^{\star} = (a_0^{\star}, a_1^{\star}, a_2^{\star}, a_3^{\star}, a_4^{\star})$ requires that all eigenvalues of $\boldsymbol{J}$ evaluated at this fixed point have negative real parts, implying that perturbations die off with time.

We now aim to stabilize the unstable fixed point $\mathbf{q}^{\star}$ corresponding to flow alignment within the range, where the system ends up in wagging motion. To this end, we use the TDFC method [31]. Following earlier work [46], we employ a diagonal control scheme, where the control force acting on the ith component (with $i = 0,1,2,3,4$) involves only the same component. Explicitly,

$$\dot{q}_i = F_i(\mathbf{q}, \boldsymbol{\beta}) - K[q_i(t) - q_i(t - \tau)], \tag{3.2}$$

where K measures the strength of control and τ is the delay time. Note that the feedback terms in Eq. (3.2) vanish when the fixed point is fully stabilized, that is, if $\mathbf{q}^{\star}(t - \tau) = \mathbf{q}^{*}(t)$. The impact of the control on the phase portrait for the two different parameter sets ($\boldsymbol{\beta}_{\mathrm{I}}, \boldsymbol{\beta}_{\mathrm{II}}$) is shown in Sec. IV.

To get a better insight into the role of the feedback control, it is instructive to perform a (linear) stability analysis of the delayed differential equations given in (3.2) [46]. In analogy to the procedure discussed before [see Eq. (A.2) below], we consider a small displacement from the fixed point $\delta \mathbf{q}(t)$. To linear order, the dynamics of this displacement follows from Eq. (3.2) as

$$\dot{\delta \mathbf{q}} = (\mathbf{J} - K \mathbf{I}) \delta \mathbf{q}(t) + K \delta \mathbf{q}(t - \tau). \tag{3.3}$$

This equation can be solved with the exponential ansatz $\delta \mathbf{q}(t) = \mathbf{B} \exp[\mu t]$, where $\mathbf{B}$ contains the amplitudes of the displacement and μ is a complex number. Inserting this ansatz into Eq. (3.3), one obtains the eigenvalue equation

$$\{\mu + K(1 - \exp[-\mu \tau])\} \delta \mathbf{q} = \mathbf{J} \delta \mathbf{q}. \tag{3.4}$$

The corresponding characteristic equation yielding the eigenvalues μ is given by

$$\det(\mathbf{J} - \{\mu + K(1 - \exp[-\mu \tau])\} \mathbf{I}) = 0. \tag{3.5}$$

However, an even simpler way to calculate the eigenvalues μ is based on the following notion: Equation (3.4) has *exactly* the same form as the corresponding equation for the uncontrolled case, Eq. (3.1). In other words, the linear operator $\mathbf{J}$ has the same set of eigenfunctions $\delta \mathbf{q}$ in both the uncontrolled and the controlled cases. This notion implies that if the eigenvalues ν of the uncontrolled system are known, then the eigenvalues μ of the controlled system can be calculated from

$$\mu + K(1 - \exp[-\mu \tau]) = \nu. \tag{3.6}$$

We also stress that Eq. (3.6) is *equivalent* to the eigenvalue equation derived in Ref. [46]. In that paper, the (diagonal) feedback control of unstable steady states in a two-dimensional dynamical system was studied from a general perspective, that is, without reference to a particular physical system. In particular, it was shown that Eq. (3.6) can be solved *analytically* by using the Lambert function $\mathcal{W}$ [55]. The same

strategy can be used in the present five-dimensional case because we are using the same diagonal control scheme. To see this, we rearrange Eq. (3.6) into

$$(\mu + K - \nu)\,\tau = K\tau \exp[-\mu\tau]. \qquad (3.7)$$

Setting $z = (\mu + K - \nu)\,\tau$ and multiplying both sides of Eq. (3.7) by $\exp[z]$, we have

$$z \exp[z] = K\tau \exp[(K - \nu)\,\tau] \equiv g. \qquad (3.8)$$

We can solve this equation with respect to z by using $z = \mathcal{W}(z \exp[z]) = \mathcal{W}(g)$. After resubstituting [i.e., $\mu\tau = z - (K - \nu)\tau$], we finally obtain the explicit formula

$$\mu\tau = \mathcal{W}(K\tau \exp[-\nu\tau + K\tau]) + \nu\tau - K\tau. \qquad (3.9)$$

We have calculated the eigenvalues both numerically [from Eq. (3.5)] and analytically [from Eq. (3.9)] for a range of control parameters K, τ for the two parameter sets $\boldsymbol{\beta}_{\mathrm{I}}$ and $\boldsymbol{\beta}_{\mathrm{II}}$ (see Figs. 1 and 2, respectively). Notice that the TDFC scheme, which is based on the coupling of a dynamical variable to its own history [see Eq. (3.2)], creates an infinite number of eigenvalues and corresponding eigenmodes [46].

IV. RESULTS

A. Fixed point stabilization in the nematic phase

We start by determining the (unstable) fixed points at the parameter set $\boldsymbol{\beta}_{\mathrm{I}}$ (see Fig. 1). Since we are in the regime of in-plane dynamic states ($a_3 = a_4 = 0$), we can visualize the nullclines of the system, i.e., the geometrical shapes where $\dot{a}_i = 0$, as two-dimensional surfaces in the three-dimensional space spanned by (a_0, a_1, a_2). These surfaces are shown in Fig. 3.

The fixed points of the system are located where all three nullclines intersect. As seen from Fig. 3, there are three fixed points (indicated by small spheres). An analysis of the corresponding Jacobian shows that all of these fixed points are unstable (i.e., at least one eigenvalue has a positive real part), as expected in the wagging regime. We remark in this context that the fixed point $\boldsymbol{q}_1^\star$ would actually be *stable* if we had restricted ourselves to the analysis of the three-dimensional system (a_0, a_1, a_2). Indeed, in this case, all three eigenvalues related to $\boldsymbol{q}_1^\star$ have negative real parts. The corresponding log-rolling state has been analyzed in Ref. [2]. In the full five-dimensional analysis, however, this fixed point becomes unstable since the nematic director can "escape" in further directions. The other fixed points, $\boldsymbol{q}_2^\star$ and $\boldsymbol{q}_3^\star$, are unstable in both the three- and the five-component dynamical systems.

Also indicated in Fig. 3 is the (stable) limit cycle emerging around the fixed point $\boldsymbol{q}_2^\star$. This limit cycle corresponds to undamped oscillations of the order parameters as functions of time. The corresponding period is close to that predicted by linear stability analysis, $T_0 = 2\pi/|\mathrm{Im}(\nu)|$, where ν is one member of the (complex conjugate) pair of eigenvalues at $\boldsymbol{q}_2^\star$ that have a positive real part (numerically, we find $\nu \approx 0.49 + i4.61$, yielding $T_0 \approx 1.36$). The dynamical evolution of an unstable configuration of dynamical variables towards the limit cycle is illustrated in Fig. 4(a). We now apply the TDFC scheme described in Sec. III B. To illustrate the impact on the phase portraits, we show in Figs. 4(b)–4(f) exemplary results
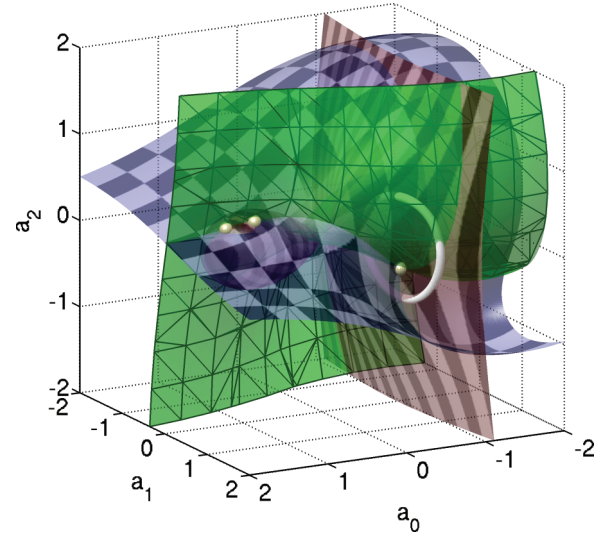

FIG. 3. (Color online) Nullclines corresponding to the dynamical variables a_0, a_1, a_2. The parameters are fixed to the set $\boldsymbol{\beta}_{\mathrm{I}}$ located within the in-plane W regime (see Fig. 1). The striped, unichrome, and checkerboard patterned surfaces are obtained from setting $\dot{a}_0 = 0$, $\dot{a}_1 = 0$, and $\dot{a}_2 = 0$, respectively (components a_3 and a_4 vanish at $\boldsymbol{\beta}_{\mathrm{I}}$). The small spheres indicate the intersections of all nullclines and thus depict the (unstable) fixed points of the system, $\boldsymbol{q}_1^\star = (1.30034, 0.139206, 0.318084, 0, 0)$, $\boldsymbol{q}_2^\star = (-0.563386, 0.807425, -0.217522, 0, 0)$, and $\boldsymbol{q}_3^\star = (0.98609, 0.232099, 0.38358, 0, 0)$. The white cycle corresponds to the stable limit cycle emerging around $\boldsymbol{q}_2^\star$.

for a fixed delay time, $\tau = 0.5$, and different values of the control strength K. All calculations have been started with the same initial values for the order parameters, a_0, a_1, a_2, and the same history regarding the onset of control. Inspecting Fig. 4, it is seen that for $K \leqslant 0.3$, the feedback control reduces the diameter of the limit cycle but the dynamics remains oscillatory at long times [see Figs. 4(b)–4(d)]. However, for $K = 0.4$ and $K = 0.5$, the initially oscillatory motion becomes more and more damped out with time, and the final state is the fixed point $\boldsymbol{q}_2^\star$. Physically, this means that the director freezes along an in-plane direction, corresponding to flow alignment. Thus, the control scheme has been successful.

A more systematic way to analyze the stability of the fixed point $\boldsymbol{q}_2^\star$ under feedback control is to monitor the complex eigenvalues μ [see Eq. (3.4)]. Specifically, we consider the largest real part of μ. Indeed, due to the transcendental character of Eq. (3.6), the spectrum of eigenvalues of the controlled system is infinite due to the infinite number of branches of the Lambert $\mathcal{W}$ function (multileaf structure). Stabilization (within the linear approximation) of the fixed point then means that $\max[\mathrm{Re}(\mu)]$ is negative at the values of K and τ considered.

To get a first insight into the ranges of control parameters where TDFC works, we plot in Fig. 5 the quantity $\max[\mathrm{Re}(\mu)]$ as a function of τ for different values of the control strength K. All curves start at the value of the real part corresponding to $\tau = 0$ where the control terms in Eq. (3.2) vanish. The positive value indicates the instability of the steady state. Upon an increase of the delay time from zero, the largest real parts corresponding to different K first decrease up to a certain
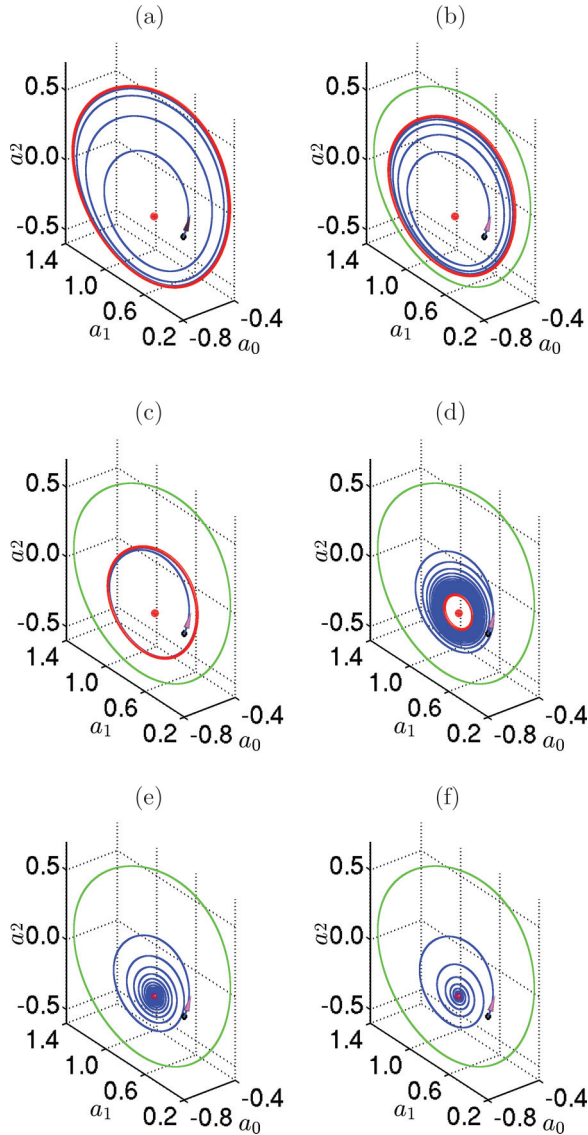
FIG. 4. (Color online) Phase portraits of the dynamical variables a_i ($i = 0, 1, 2$). Parameters are fixed to the set $\boldsymbol{\beta}_I$ located within the in-plane W regime (see Fig. 1). The central small red dot marks the (unstable) fixed point. (a) Uncontrolled system ($K = 0$) with the initial condition $a_0^{\text{init}} = -0.57$, $a_1^{\text{init}} = 0.5$, $a_2^{\text{init}} = -0.22$. The initial condition is indicated with a black diamond. (b)–(f) Systems under time-delayed feedback control [see Eq. (3.2)] with control strength (b) $K = 0.1$, (c) 0.2, (d) 0.3, (e) 0.4, and (f) 0.5, respectively, and delay time $\tau = 0.5$. In all cases in (b)–(f), the control starts at $t = 0$, assuming that $a_i(t) = a_i^{\text{init}}$ in the interval $[-\tau, 0]$. In (a)–(d) the blue (dark gray) trajectories approach stable limit cycles, which are plotted as thick red (medium gray) cycles. In (b)–(f) the limit cycle of the uncontrolled system in (a) is replotted for reference as a green (light gray) cycle. For (e) and (f) the trajectories end at the fixed point.

delay time and subsequently display an oscillatory behavior. However, for the cases $K = 0.1$ and $K = 0.2$, the largest real part remains positive. Only for $K \geqslant 0.3$ do values of τ where the largest real parts become negative exist, indicating that the control is successful.
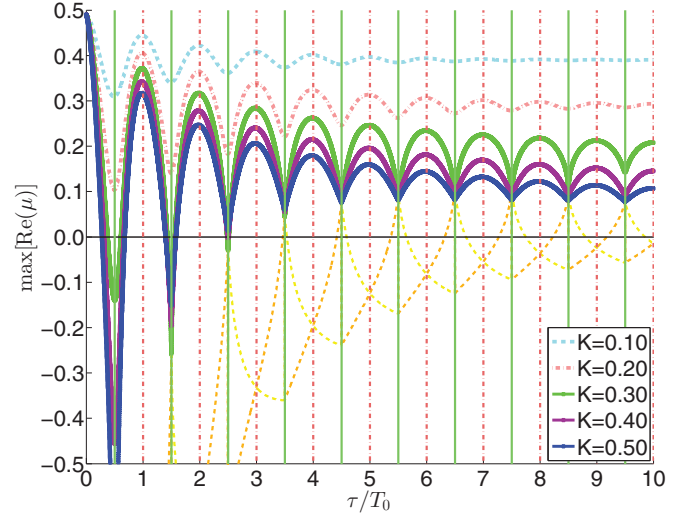

FIG. 5. (Color online) Largest real part of the complex eigenvalues μ vs τ for different values of K. The dot-dashed vertical lines correspond to multiples of $T_0 = 2\pi/|\text{Im}(\nu)|$ ($T_0 \approx 1.36$), where ν is the eigenvalue of the uncontrolled system at the fixed point $\boldsymbol{q}_2^\star$ (see Fig. 3). The solid vertical lines are shifted relative to the dashed lines by $T_0/2$. The dashed lines in the lower part indicate some lower branches of eigenvalues for $K = 0.30$. The other parameters are fixed to the set $\boldsymbol{\beta}_I$ located within the in-plane W regime (see Fig. 1).

Following the analysis in Ref. [46], it is possible to analytically determine the minimum value of K required to control the system at specific values of τ. The boundary of stability is determined by the condition $\text{Re}(\mu) = 0$, or equivalently, $\mu = i\Omega$ (with Ω being real). Inserting this into Eq. (3.6), we find

$$\text{Re}(\nu) = K(1 - \cos \Omega\tau),$$
$$\text{Im}(\nu) = \Omega + K \sin \Omega\tau. \tag{4.1}$$

From the first equation in Eq. (4.1) it follows that at the boundary of stability, K varies between $\text{Re}(\nu)/2$ and ∞ (since $\cos \Omega\tau$ is bounded between -1 and 1). Thus, the minimal value of K is given by

$$K_{\min} = \text{Re}(\nu)/2, \tag{4.2}$$

corresponding to $\cos \Omega\tau = -1$. The fixed point $\boldsymbol{q}_2^\star$ considered here is characterized by $\text{Re}(\nu) \approx 0.49$, yielding $K_{\min} \approx 0.25$ according to Eq. (4.2). This is consistent with the results displayed in Fig. 5. We can also obtain a constraint for the delay times corresponding to the stability boundary. Specifically, the condition $\cos \Omega\tau = -1$ requires that

$$\Omega\tau = (2n + 1)\pi, \quad n = 0, 1, 2, \dots, \tag{4.3}$$

Equation (4.3) immediately implies that $\sin \Omega\tau = 0$. From the second equation of Eq. (4.1) it therefore follows that $\Omega = \text{Im}(\nu)$. Combining this with Eq. (4.3), we obtain the following condition for the delay times at minimum K:

$$\tau = \frac{\pi}{\text{Im}(\nu)}(2n + 1)$$
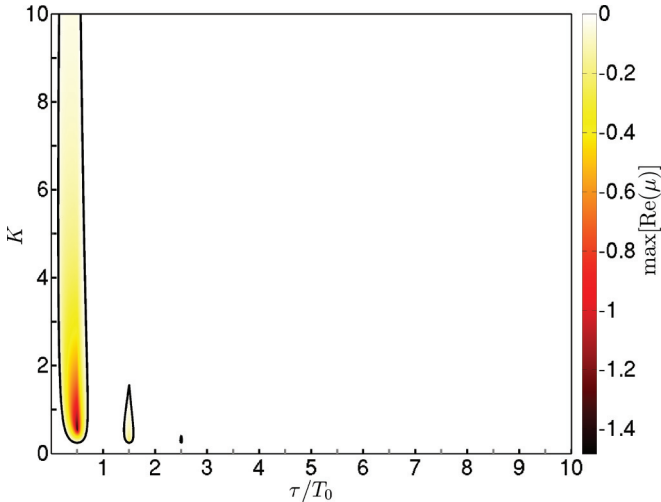$$= T_0\left(n + \frac{1}{2}\right), \quad n = 0, 1, 2, \dots, \tag{4.4}$$

FIG. 6. (Color online) Largest real part of the complex eigenvalues μ in the K-τ plane (only negative values are shown). The black contours bound regions where the largest real part is negative. The shear parameters are fixed to the set $\boldsymbol{\beta}_{\mathrm{I}}$ located within the in-plane W regime (see Fig. 1).

FIG. 7. (Color online) Same as Fig. 3, but for the parameter set $\boldsymbol{\beta}_{\mathrm{II}}$ located within the island of W dynamics, which appears on shearing from the isotropic phase (see Fig. 2). The small sphere indicates the unstable fixed point, $\boldsymbol{q}^{*}_{1} = [-0.283501, 0.49587, 0.108511, 0, 0]$. The white cycle corresponds to the stable limit cycle emerging around $\boldsymbol{q}^{\star}_{1}$.

where we have used $T_0 = 2\pi/|\mathrm{Im}(\nu)|$. We conclude that both of the control parameters, K and τ, required to stabilize the fixed point are intimately related to the eigenvalues of the uncontrolled system

A further interesting case occurs when $\cos \Omega\tau = 1$ in Eq. (4.1). In this case, control is essentially impossible since the corresponding value of the control strength [at finite values of $\mathrm{Re}(\nu)$] is $K = \infty$. The corresponding delay times can be found using the same arguments as those leading to Eq. (4.4). Specifically, one has $\sin \Omega\tau = 0$ [and thus $\Omega = \mathrm{Im}(\nu) = 2\pi/T_0$], but this time $\Omega\tau$ is an even multiple of π [contrary to Eq. (4.3)]. We therefore find that at delay times $\tau = nT_0$ with $n = 0, 1, 2, \ldots$, stabilization via TDFC is not possible for any finite value of K. The important role of the delay time is reflected in Fig. 5. For all values of K considered, we find the minima of the functions $\max[\mathrm{Re}(\mu)]$ to occur at $\tau = (n + 1/2)T_0$, while maxima occur at even multiples of T_0. Further (analytic) results on the domain of control in the (K, τ) plane can be found in Ref. [46], where the same diagonal control scheme has been employed to stabilize a fixed point.

So far we have focused on some specific values of K. To get an overall "stability map" we show in Fig. 6 the real part of the largest eigenvalue in the K-τ plane (only negative values are plotted). The black contours indicate the control parameters where the real part of the largest eigenvalue becomes zero. Within the black contours the real part is negative (colored in the plot); therefore these lines bound the regions where TDFC is successful. It is seen that the areas of stabilization shrink with increasing delay time and eventually disappear. This is due to the scaling behavior of the eigenvalue spectrum for large τ [56,57].

B. Stabilization in the isotropic phase

As a second example for the stabilization of a fixed point we now consider the reduced temperature $\theta = 1.20$, at which
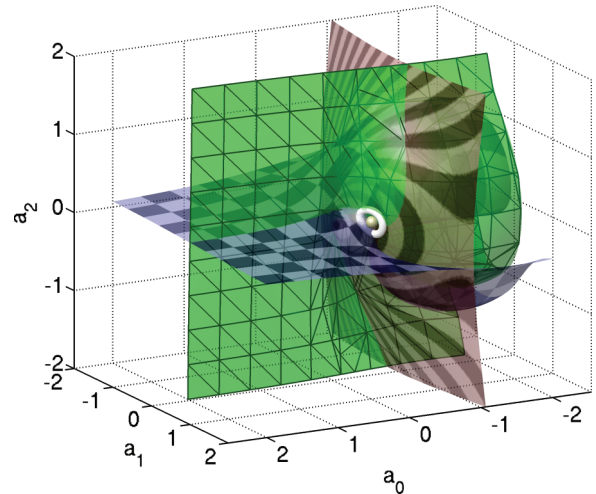
the equilibrium (i.e., zero-shear) system is orientationally disordered. The presence of shear then induces either flow alignment or oscillatory dynamics (of type W). As seen from Fig. 2, stable W motion occurs at rather small values of the coupling parameter λ_K and intermediate values of the shear rate. Within this "island" of W motion, we now focus on the parameter set $\boldsymbol{\beta}_{\mathrm{II}}$. The corresponding nullclines (pertaining to the components a_0, a_1, and a_2) are shown in Fig. 7. Contrary to the situation within the nematic phase discussed in the previous paragraph, we find at $\boldsymbol{\beta}_{\mathrm{II}}$ only one (unstable) fixed point, $\boldsymbol{q}^{*}_{1}$, and one stable limit cycle. The relevant eigenvalue of the uncontrolled system at the fixed point is given by $\nu \approx 0.027 + i0.65$. From that, we find the oscillation period $T_0 = 2\pi/|\mathrm{Im}(\nu)| \approx 9.68$.

In Fig. 8(a) we replot this limit cycle, supplemented by phase portraits illustrating the impact of TDFC. It is seen that the feedback control has a significant effect already at very small values of the control strength, that is, at $K = 0.03$, although the chosen time delay is rather large ($\tau = 5.0$). This already indicates that the system reacts more sensitively to TDFC compared to the system considered before.

The fact that small K are sufficient to stabilize the fixed point is supported by the behavior of the largest real part of the eigenvalue μ plotted as a function of τ in Fig. 9. Clearly, the functions have the same qualitative behavior as those obtained in the nematic phase (see Fig. 5); however, the numerical values of K are much smaller.

Finally, we present in Fig. 10 the ranges of control parameters where TDFC is successful; the boundaries have again been obtained from Eqs. (4.2) and (4.4), respectively. Compared to the nematic system, we observe a much larger number of areas where the fixed point can be stabilized. This underlines our finding that less effort is required to stabilize liquid-crystalline systems sheared from the isotropic phase than systems sheared from the nematic phase.
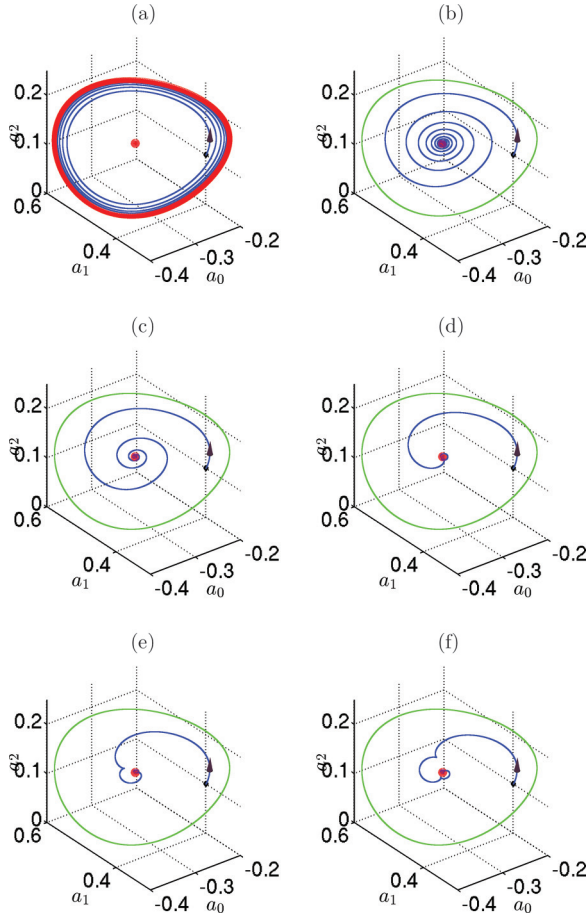
FIG. 8. (Color online) Phase portraits of the dynamical variables a_i ($i = 0,1,2$). The central small dot marks the (unstable) fixed point. (a) Uncontrolled system ($K = 0$) with initial condition $a_0^{\text{init}} = -0.20$, $a_1^{\text{init}} = 0.4$, $a_2^{\text{init}} = 0.1$. (b)–(f) Systems under time-delayed feedback control [see Eq. (3.2)] with the control strength (b) $K = 0.03$, (c) 0.05, (d) 0.1, (e) 0.15, and (f) 0.2, respectively, and delay time $\tau = 5.0$. In all cases in (b)–(f), the control starts at $t = 0$, assuming that $a_i(t) = a_i^{\text{init}}$ in the interval $[-\tau,0]$. In (a) the blue (dark gray) trajectory approaches a stable limit cycle, which is plotted as a thick red (medium gray) cycle. In (b)–(f) the limit cycle of the uncontrolled system in (a) is replotted for reference as a green (light gray) cycle. For (b)–(f) all trajectories end in the fixed point. The shear parameters are fixed to the set $\boldsymbol{\beta}_{\text{II}}$; see Fig. 2.

V. CONCLUSIONS

In the present paper we have discussed a five-dimensional dynamical system describing the director dynamics of sheared liquid crystal under time-delayed feedback control. The goal was to stabilize the stationary, flow-aligned state for shear rates and shear coupling parameters, where the uncontrolled system performs an oscillatory wagging motion in the shear plane. To this end we have applied a diagonal feedback control scheme involving a single delay time τ. Following earlier theoretical work [46], we have analytically studied the (linear) stability problem of the controlled system, yielding explicit expressions for the domain of control. One main result is that the *optimal* values of control strength and delay time are closely related to the relevant complex eigenvalue of the
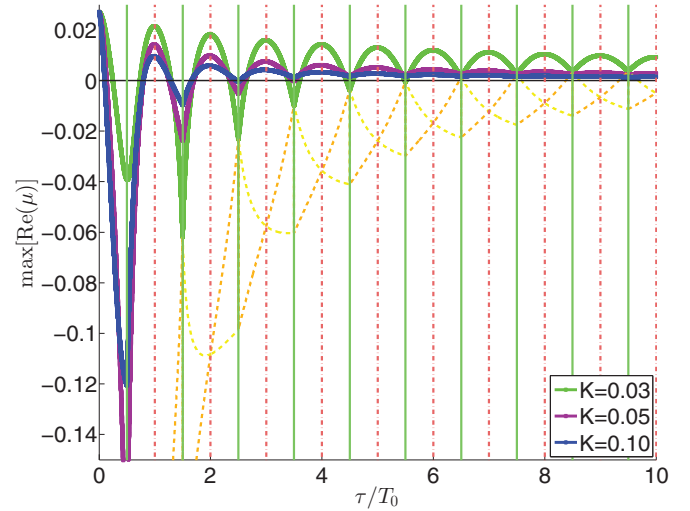

FIG. 9. (Color online) Largest real part of the complex eigenvalues μ vs τ for different values of K (the shear parameters are fixed to the set $\boldsymbol{\beta}_{\text{II}}$; see Fig. 2). The dash-dotted vertical lines correspond to multiples of $T_0 = 2\pi/|\text{Im}(\nu)|$ ($T_0 \approx 9.68$), where ν is the eigenvalue of the uncontrolled system at the fixed point $\boldsymbol{q}_1^{\star}$ (see Fig. 7). The solid vertical lines are shifted relative to the dash-dotted lines by $T_0/2$. The dashed lines in the lower part indicate some lower branches of eigenvalues for $K = 0.03$.

corresponding uncontrolled system, that is, the sheared liquid crystal in the wagging state. Interestingly, there is also a strong influence of the equilibrium state from which the system was sheared: in a system sheared from the isotropic phase, the control strength required to stabilize flow alignment is much smaller than in a sheared nematic system. This shows that interaction effects between the particles (which are responsible for the isotropic-nematic transition) are crucially important.

From a more general perspective, the present study thus shows that TDFC of unstable steady states, which has already
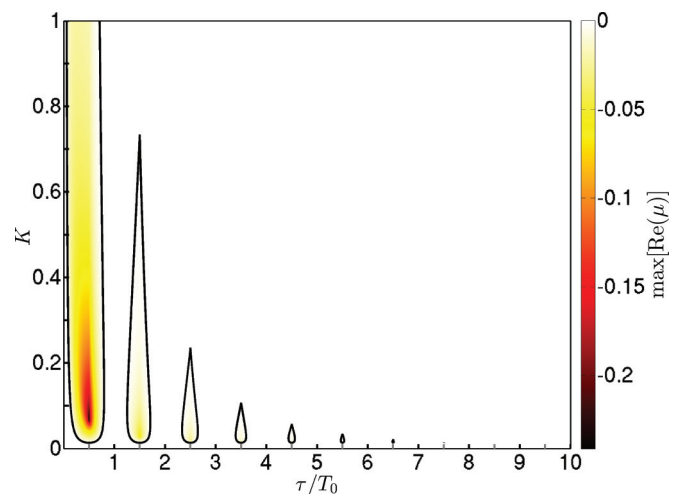

FIG. 10. (Color online) Largest real part of the complex eigenvalues μ in the K-τ plane. The black contours bound regions where the largest real part is negative; these regions are colored according to the color map. The shear parameters are fixed to the set $\boldsymbol{\beta}_{\text{II}}$; see Fig. 2.

been applied to a variety of optical and neural systems [37,42,58,59] is also possible and useful in the context of nonequilibrium soft-matter systems such as sheared complex fluids. In that case, stabilization of the flow-aligned state seems particularly interesting because flow alignment is characterized by a small shear viscosity (as opposed to that of oscillatory states). Nevertheless, from a fundamental point of view it would be very interesting to extend the present analysis to the (time-delayed) feedback control of oscillatory states, which are also observed experimentally (e.g., in suspensions of tobacco viruses) [16,60]. Of course, these considerations prompt the question how a closed-loop feedback scheme such as the one proposed here could be realized experimentally.

In that context we would like to note that the control targets chosen in our study, that is, the components of the order parameter tensor $\mathbf{a}(t)$, are related to material properties accessible in experiments. In particular, the components a_1 and a_2 are related to the so-called flow angle [24] (i.e., the angle between the nematic director and the flow direction) and to birefringence [61–63]. Moreover, there is a direct relation between the alignment and the stress tensor, which can be measured in rheological experiments. This offers an additional route to extract at least some (typically nondiagonal) components of $\mathbf{a}$. Given that it can be difficult to monitor all components of $\mathbf{a}$ at once, the present diagonal control scheme, where all a_i $(i = 0, \ldots, 4)$ are treated on the same footing, may seem too artificial. We note, however, that the control scheme could be easily modified such that only some experimentally accessible components of $\mathbf{a}$ are controlled (see Ref. [64] for an application in a laser with feedback). The only drawback is that an analytical treatment is then impossible.

We further note that *additive* terms, such as the control terms in our TDFC scheme, also arise if the system is under the influence of an external (magnetic or electrical) field. For example, a magnetic field $\boldsymbol{H}$ would lead to an additional free energy contribution of the form $\Phi = -\boldsymbol{H} \cdot \boldsymbol{a} \cdot \boldsymbol{H}$, yielding additive terms $\propto H^2$ in the equation of motion [see Eq. (2.5)]. One idea could therefore be to choose the strength of the external field, or, rather, of H^2, to be linearly dependent on the order parameters to generate a linear control scheme such as the one used here. Further possibilities to detect, and thus to control, the orientational motion could arise if the particles carry electric or magnetic moments on their own, such that time-dependent director motion directly leads to electromagnetic fields. Theoretically, the dynamical properties of such systems (without feedback control) have already been investigated [48].

ACKNOWLEDGMENTS

APPENDIX

The components of vector $\boldsymbol{\Phi}$ [consists of projections of $\Phi'(\boldsymbol{a})$ on to the tensor basis] are as follows:

$$\phi_0 = (\theta - 3a_0 + 2a^2)a_0 + 3(a_1^2 + a_2^2) - \tfrac{3}{2}(a_3^2 + a_4^2),$$

$$\phi_1 = (\theta + 6a_0 + 2a^2)a_1 - \tfrac{3}{2}\sqrt{3}(a_3^2 - a_4^2),$$

$$\phi_2 = (\theta + 6a_0 + 2a^2)a_2 - 3\sqrt{3}a_3a_4, \qquad \text{(A1)}$$

$$\phi_3 = (\theta - 3a_0 + 2a^2)a_3 - 3\sqrt{3}(a_1a_3 + a_2a_4),$$

$$\phi_4 = (\theta - 3a_0 + 2a^2)a_4 - 3\sqrt{3}(a_2a_3 - a_1a_4).$$

See also Refs. [22,24,27].

The elements of the Jacobian, $J_{ij} = \partial F_i / \partial q_j$, are given by

$$J_{00} = -(\theta - 6a_0 + 4a_0^2 + 2a^2), \qquad \text{(A2)}$$

$$J_{01} = -(4a_0a_1 + 6a_1), \qquad \text{(A3)}$$

$$J_{02} = -(4a_0a_2 + 6a_2), \qquad \text{(A4)}$$

$$J_{03} = -(4a_0a_3 - 3a_3), \qquad \text{(A5)}$$

$$J_{04} = -(4a_0a_4 - 3a_4), \qquad \text{(A6)}$$

$$J_{10} = -[(6 + 4a_0)a_1], \qquad \text{(A7)}$$

$$J_{11} = -(\theta + 6a_0 + 2a^2 + 4a_1^2), \qquad \text{(A8)}$$

$$J_{12} = -(4a_1a_2) + \dot{\gamma}, \qquad \text{(A9)}$$

$$J_{13} = -(4a_1a_3 - 3\sqrt{3}a_3), \qquad \text{(A10)}$$

$$J_{14} = -(4a_1a_4 + 3\sqrt{3}a_4), \qquad \text{(A11)}$$

$$J_{20} = -[(6 + 4a_0)a_2], \qquad \text{(A12)}$$

$$J_{21} = -(4a_1a_2) - \dot{\gamma}, \qquad \text{(A13)}$$

$$J_{22} = -(\theta + 6a_0 + 2a^2 + 4a_2^2), \qquad \text{(A14)}$$

$$J_{23} = -(4a_2a_3 - 3\sqrt{3}a_4), \qquad \text{(A15)}$$

$$J_{24} = -(4a_2a_4 - 3\sqrt{3}a_3), \qquad \text{(A16)}$$

$$J_{30} = -[(-3 + 4a_0)a_3], \qquad \text{(A17)}$$

$$J_{31} = -(4a_1a_3 - 3\sqrt{3}a_3), \qquad \text{(A18)}$$

$$J_{32} = -(4a_2a_3 - 3\sqrt{3}a_4), \qquad \text{(A19)}$$

$$J_{33} = -[4a_3^2 - 3\sqrt{3}a_1 + (\theta - 3a_0 + 2a^2)], \quad \text{(A20)}$$

$$J_{34} = -(4a_4a_3 - 3\sqrt{3}a_2) + \tfrac{1}{2}\dot{\gamma}, \qquad \text{(A21)}$$

$$J_{40} = -[(-3 + 4a_0)a_4], \qquad \text{(A22)}$$

$$J_{41} = -(4a_1a_4 + 3\sqrt{3}a_4), \qquad \text{(A23)}$$

$$J_{42} = -(4a_2a_4 - 3\sqrt{3}a_3), \qquad \text{(A24)}$$

$$J_{43} = -(4a_3a_4 - 3\sqrt{3}a_2) - \tfrac{1}{2}\dot{\gamma}, \qquad \text{(A25)}$$

$$J_{44} = -[4a_4^2 + 3\sqrt{3}a_1 + (\theta - 3a_0 + 2a^2)]. \quad \text{(A26)}$$

[1] G. Rienäcker, M. Kröger, and S. Hess, Phys. Rev. E **66**, 040702(R) (2002).

[2] G. Rienäcker, M. Kröger, and S. Hess, Phys. A **315**, 537 (2002).

[3] M. Grosso, S. Crescitelli, E. Somma, J. Vermant, P. Moldenaers, and P. L. Maffettone, Phys. Rev. Lett. **90**, 098304 (2003).

[4] M. G. Forest, Q. Wang, and R. Zhou, Rheol. Acta **86**, 80 (2004).

[5] M. Ripoll, P. Holmqvist, R. G. Winkler, G. Gompper, J. K. G. Dhont, and M. P. Lettinga, Phys. Rev. Lett. **101**, 168302 (2008).

[6] M. Das, B. Chakrabarti, C. Dasgupta, S. Ramaswamy, and A. K. Sood, Phys. Rev. E **71**, 021707 (2005).

[7] S. Hess, Z. Naturforsch. **30a**, 728 (1975).

[8] S. Hess, Z. Naturforsch. **31a**, 1034 (1976).

[9] M. Doi, Ferroelectrics **30**, 247 (1980).

[10] M. Doi, J. Polym. Sci. Polym. Phys. Ed. **19**, 229 (1981).

[11] P. D. Olmsted and P. M. Goldbart, Phys. Rev. A **46**, 4966 (1992).

[12] Y.-G. Tao, W. K. den Otter, and W. J. Briels, Phys. Rev. Lett. **95**, 237802 (2005).

[13] Y. Tao, W. den Otter, and W. Briels, Europhys. Lett. **86**, 56005 (2009).

[14] G. Germano and F. Schmid, J. Chem. Phys. **123**, 214703 (2005).

[15] R. Bandyopadhyay, G. Basappa, and A. K. Sood, Phys. Rev. Lett. **84**, 2022 (2000).

[16] M. P. Lettinga, Z. Dogic, H. Wang, and J. Vermant, Langmuir **21**, 8048 (2005).

[17] S. M. Fielding, Soft Matter **3**, 1262 (2007).

[18] A. Aradian and M. E. Cates, Europhys. Lett. **70**, 397 (2005).

[19] M. E. Cates, D. A. Head, and A. Ajdari, Phys. Rev. E **66**, 025202(R) (2002).

[20] A. Aradian and M. E. Cates, Phys. Rev. E **73**, 041508 (2006).

[21] C. Goddard, O. Hess, A. G. Balanov, and S. Hess, Phys. Rev. E **77**, 026311 (2008).

[22] S. H. L. Klapp and S. Hess, Phys. Rev. E **81**, 051711 (2010).

[23] S. Heidenreich, S. Hess, and S. H. L. Klapp, Phys. Rev. Lett. **102**, 028301 (2009).

[24] S. Hess and M. Kröger, J. Phys. Condensed Matter **16**, S3835 (2004).

[25] D. A. Strehober, E. Schöll, and S. H. L. Klapp, in *9th International Conference on Mathematical Problems in Engineering, Aerospace and Sciences: ICNPAA 2012*, AIP Conf. Proc. No. 1493 (AIP, New York, 2012), p. 552.

[26] G. Rienäcker, Ph.D. thesis, TU Berlin, 2000.

[27] D. A. Strehober, H. Engel, and S. H. L. Klapp, Phys. Rev. E **88**, 012505 (2013).

[28] L. R. P. de Andrade Lima and A. D. Rey, Phys. Rev. E **70**, 011701 (2004).

[29] T. Tsuji and A. D. Rey, J. Non-Newtonian Fluid Mech. **73**, 127 (1997).

[30] A. D. Rey and M. M. Denn, Annu. Rev. Fluid Mech. **34**, 233 (2002).

[31] K. Pyragas, Phys. Lett. A **170**, 421 (1992).

[32] N. Baba, A. Amann, E. Schöll, and W. Just, Phys. Rev. Lett. **89**, 074101 (2002).

[33] J. Unkelbach, A. Amann, W. Just, and E. Schöll, Phys. Rev. E **68**, 026204 (2003).

[34] J. Schlesner, A. Amann, N. B. Janson, W. Just, and E. Schöll, Phys. Rev. E **68**, 066208 (2003).

[35] M. Kehrt, P. Hövel, V. Flunkert, M. A. Dahlem, P. Rodin, and E. Schöll, Eur. Phys. J. B **68**, 557 (2009).

[36] T. Dahms, P. Hövel, and E. Schöll, Phys. Rev. E **78**, 056213 (2008).

[37] T. Dahms, V. Flunkert, F. Henneberger, P. Hövel, S. Schikora, E. Schöll, and H. J. Wünsche, Eur. Phys. J. Spec. Top. **191**, 71 (2010).

[38] J. Schlesner, V. Zykov, H. Engel, and E. Schöll, Phys. Rev. E **74**, 046215 (2006).

[39] J. Schlesner, V. S. Zykov, H. Brandstädter, I. Gerdes, and H. Engel, New J. Phys. **10**, 015003 (2008).

[40] Y. N. Kyrychko, K. B. Blyuss, S. J. Hogan, and E. Schöll, Chaos **19**, 043126 (2009).

[41] M. A. Dahlem, F. M. Schneider, and E. Schöll, Chaos **18**, 026110 (2008).

[42] E. Schöll, G. Hiller, P. Hövel, and M. A. Dahlem, Philos. Trans. R. Soc. A **367**, 1079 (2009).

[43] A. Panchuk, D. P. Rosin, P. Hövel, and E. Schöll, Bifurcation Chaos Appl. Sci. Eng. **23**, 1330039 (2013).

[44] *Handbook of Chaos Control*, edited by E. Schöll and H. G. Schuster (Wiley VCH, Weinheim, 2008).

[45] E. Schöll, *Nonlinear Dynamics of Nanosystems*, edited by G. Radons, B. Rumpf, and H. G. Schuster (Wiley-VCH, Weinheim, 2009).

[46] P. Hövel and E. Schöll, Phys. Rev. E **72**, 046203 (2005).

[47] A. Sonnet, A. Kilian, and S. Hess, Phys. Rev. E **52**, 718 (1995).

[48] S. Grandner, S. Heidenreich, S. Hess, and S. H. L. Klapp, Eur. Phys. J. E **24**, 353 (2007).

[49] S. Hess and M. Kröger, in *Computer Simulations of Liquid Crystals and Polymers*, NATO Science Series II: Mathematics, Physics and Chemistry Vol. 177, edited by P. Pasini, C. Zannoni, and S. Zumer (Springer, Dordrecht, 2005), pp. 295–333.

[50] S. Grandner, S. Heidenreich, S. Hess, and S. H. L. Klapp, Eur. Phys. J. E **24**, 353 (2007).

[51] S. Grandner, S. Heidenreich, P. Ilg, S. Klapp, and S. Hess, Phys. Rev. E **75**, 040701(R) (2007).

[52] P. G. de Gennes and J. Prost, *The Physics of Liquid Crystals* (Clarendon, Oxford, 1993).

[53] S. Heidenreich, Ph.D. thesis, TU Berlin, 2008.

[54] R. G. Larson and H. C. Öttinger, Macromolecules **24**, 6270 (1991).

[55] R. M. Corless, G. H. Gonnet, D. E. G. Hare, D. J. Jeffrey, and D. E. Knuth, Adv. Comput. Math. **5**, 329 (1996).

[56] S. Yanchuk, M. Wolfrum, P. Hövel, and E. Schöll, Phys. Rev. E **74**, 026201 (2006).

[57] M. Wolfrum, S. Yanchuk, P. Hövel, and E. Schöll, Eur. Phys. J. Spec. Top. **191**, 91 (2010).

[58] J. Lehnert, P. Hövel, V. Flunkert, P. Y. Guzenko, A. L. Fradkov, and E. Schöll, Chaos **21**, 043111 (2011).

[59] P. Hövel, M. A. Dahlem, and E. Schöll, Int. J. Bifurcation Chaos Appl. Sci. Eng. **20**, 813 (2010).

[60] M. P. Lettinga and J. K. G. Dhont, J. Phys. Condens. Matter **16**, S3929 (2004).

[61] W. R. Burghardt, Macromol. Chem. Phys. **199**, 471 (1998).

[62] M. L. Kilfoil and P. T. Callaghan, Macromolecules **33**, 6828 (2000).

[63] J. Cao and B. J. Berne, J. Chem. Phys. **99**, 2213 (1993).

[64] V. Flunkert and E. Schöll, Phys. Rev. E **84**, 016214 (2011).